Original Paper

phys. stat. sol. (b) **243**, No. 13, 3359–3364 (2006) / **DOI** 10.1002/pssb.200669130

Electrical transport measurements of nanotubes with known (*n*, *m*) indices

Bhupesh Chandra[1], **Robert Caldwell**[2], **Mingyuan Huang**[1], **Limin Huang**[2], **Matthew Y. Sfeir**[3], **Stephen P. O'Brien**[2], **Tony F. Heinz**[3], and **James Hone**[*, 1]

[1] Department of Mechanical Engineering, Nanoscale Science and Engineering Center, Columbia University, New York, NY 10027, USA
[2] Department of Applied Physics, Nanoscale Science and Engineering Center, Columbia University, New York, NY 10027, USA
[3] Department of Electrical Engineering, Nanoscale Science and Engineering Center, Columbia University, New York, NY 10027, USA

Received 24 April 2006, revised 24 May 2006, accepted 1 August 2006
Published online 19 September 2006

PACS 61.46.Fg, 73.63.Fg, 81.07.De

Because subtle changes in physical structure (chirality) can cause the electronic structure of carbon nanotubes to vary from metallic to semiconducting, the goal of fully controlled nanotube device fabrication has proved elusive. Using a mechanical transfer technique in parallel with optical characterization, we have achieved the goal of placing 'the nanotube we want, where we want it'. Long nanotubes are grown by CVD across a slit etched through a Si wafer and then examined by Rayleigh scattering. By combining this technique with structural characterization by electron diffraction, we are able to map each spectrum to a unique (*n*, *m*) structure. After structural characterization, a chosen nanotube can be transferred to a substrate in the desired location, and devices fabricated using standard e-beam lithography techniques. We have fabricated a number of devices in this manner and are beginning to fully explore the detailed relationship between structure and transport.

1 Introduction

Soon after the discovery of carbon nanotubes in 1991, it was realized that their electronic properties should be highly sensitive to their geometry, as defined by their chiral vector (*n*, *m*) [1]. Specifically, a tight-binding, single-electron model predicts that nanotubes with $(n - m) = 3i$, where i is an integer, are metals, whereas all others are semiconductors with bandgaps varying inversely with diameter (of order 0.5–1 eV for SWNTs in the 1–2 nm diameter range). Refinements to this model predict that only armchair (*n*, *n*) tubes are truly metals, while the other metals should exhibit small curvature-induced gaps of order tens of meV [2]. These theoretical predictions have been verified in a number of ways. In particular, scanning tunnelling spectroscopy (STS) combined with STM imaging has provided tunneling spectra on nanotubes of known structure [3].

A detailed understanding of the electrical transport properties of nanotubes is important for many applications. In particular, because of the diameter dependence of the semiconducting gap, the performance of nanotube FETs should depend strongly on diameter [4]. Electron–phonon scattering is also strongly diameter-dependent [5]. Finally, electromechanical effects in nanotubes should be highly sensitive to both diameter and chirality [6]. A few studies have shown initial success toward combining elec-

[*] Corresponding author: e-mail: jh2228@columbia.edu, Phone: +01 212 854 6244, Fax: +01 212 854 3304

trical transport with structural probes such as Raman spectroscopy [7], TEM imaging [8], and electron diffraction [9]. However, the geometry required for such studies (typically a freely-suspended nanotube) imposes limitations on the type and configuration of electronic leads that can be attached, and in general makes sample fabrication difficult. Below we describe a technique that separates the problems of structural characterization and electrical measurements by mechanical transfer of freely suspended nanotubes to standard substrates, and show initial results.

2 Nanotube growth and characterization

Figure 1 depicts the growth and characterization of the samples used in this work. First, slits (typically 100 μm wide and 1 mm long) are etched through Si wafers by standard bulk micromachining techniques. Next, catalyst is placed at one end of the wafer. Catalysts used for this work include silica-supported Co/Mo, and thin (1 nm) Co films [10]. Nanotubes are then grown by atmospheric pressure chemical vapor deposition (CVD) at 850–900 °C, using ethanol as a feedstock. This growth typically yields a significant number (of order 10) of long SWNTs that extend mm distances from the catalyst. These long tubes cross the slit, resulting in freely suspended sections that can be characterized by multiple techniques.

Optical spectroscopy techniques, such as flourescence or Raman scattering, have been shown to be powerful tools for characterization of nanotubes. The suspended structures shown above are particularly well-suited to optical characterization due to the lack of background signal from a substrate. In this study, the nanotubes are characterized primarily by Rayleigh scattering spectroscopy [11]. In this technique, optical transitions in the nanotube appear as peaks in the scattering spectrum. Rayleigh scattering works for every type of nanotube, whereas fluorescence only works for semiconducting tubes. Also, the technique is fast and does not require a tunable laser source, as is required for resonance Raman scattering. Rayleigh scattering can also easily distinguish single tubes from bundles, and can examine the structure at multiple points along the tube.

Tight-binding theory indicates that every nanotube should display a series of optical transitions that directly reflects the peaks in the 1D density of electronic states. Furthermore, because of the angular dependence of the graphene energy dispersion relation (the trigonal warping effect), measurement of two or more of these transitions should provide a unique fingerprint for each nanotube. Both fluorescence [12] and resonance Raman scattering [13] have been used for index assignment in this way. However, it

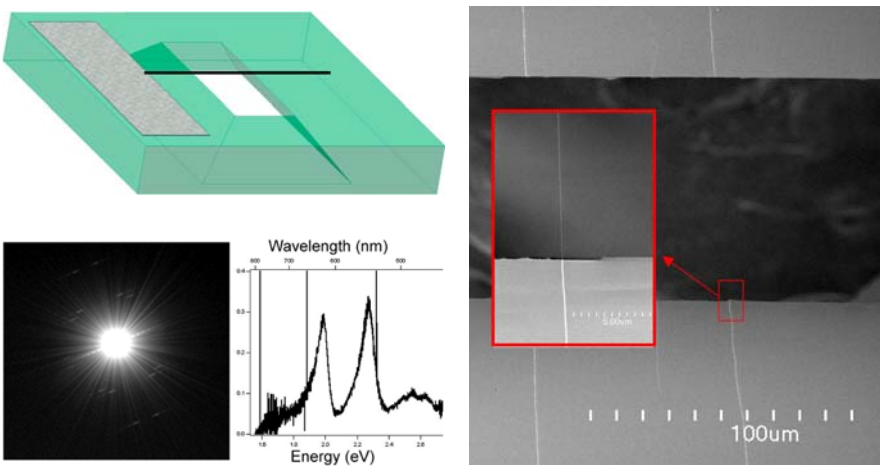

Fig. 1 (online colour at: www.pss-b.com) Suspended nanotube structrures. Top left, schematic diagram of long nanotube, growing from catalyst at left, extending across slit. Right, SEM images of nanotubes crossing a slit. Bottom left, electron diffraction pattern and Rayleigh scattering spectrum of a (16, 11) tube.

should be noted that single-electron tight binding theory does not accurately predict the absolute optical transition energies in nanotubes, although it seems to predict the general pattern of transition energie correctly. To provide a solid experimental foundation for our index assignment, we have, in a separate study, used TEM electron diffraction for independent determination of the structure (Fig. 1, bottom left) of ~10 tubes, which significantly constrains the index assignment problem [14].

For the samples used in this work, index assignment was done purely by Rayleigh spectroscopy. The assignment scheme is as follows. First, the nanotube is classified as armchair ($n = m$, single peak), chiral metal ($n - m = 3i$, split peak), or semiconducting ($n - m \neq 3i$, two separate peaks). Next, the diameter is assigned by measuring the position of the single peak or the average position of the two peaks. For both metals and semiconductors, we have observed that this quantity scales inversely with tube diameter in a few samples of known structure. Finally, the chiral angle can be assigned by measuring the separation between the peaks, which increases as the chiral angle deviates from the armchair direction. Although we cannot yet conclusively assign indices to every spectrum, all of the nanotubes shown below are close in structure to previously identified tubes, and therefore their structure can be assigned by straightforward interpolation. Ongoing measurements will provide additional data points for assignment.

3 Nanotube transfer and device fabrication

Although the suspended nanotube geometry is ideal for optical characterization, it is highly inconvenient for transport measurements. Therefore, we have devised a method, depicted in Fig. 2, for mechanical transfer of the suspended nanotube to a solid substrate [15]. After optical characterization, a nanotube with the desired characteristics is chosen, and all of the other nanotubes crossing the slit are burned away with a laser (because the nanotubes are generally spaced ~50–100 microns apart, this does not damage the chosen tube). Using a contact mask aligner, the growth chip is then placed upside down on another ('target') chip, such that the suspended nanotube section touches the target chip between pre-defined

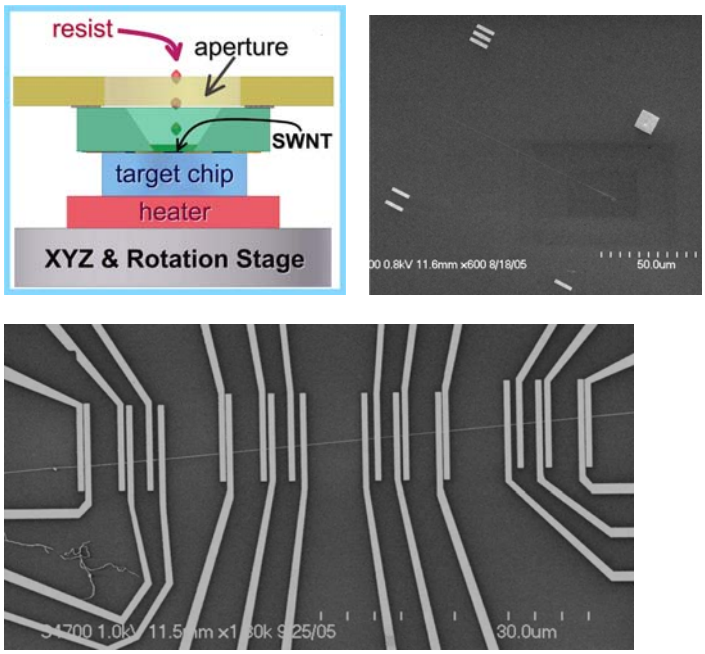

Fig. 2 (online colour at: www.pss-b.com) Nanotube transfer and device fabrication. Top left, setup for mechanical transfer of suspended nanotubes to target chip. Top right, transferred nanotube between alignment marks. Bottom, transferred nanotube with electrical leads defined by e-beam lithography.

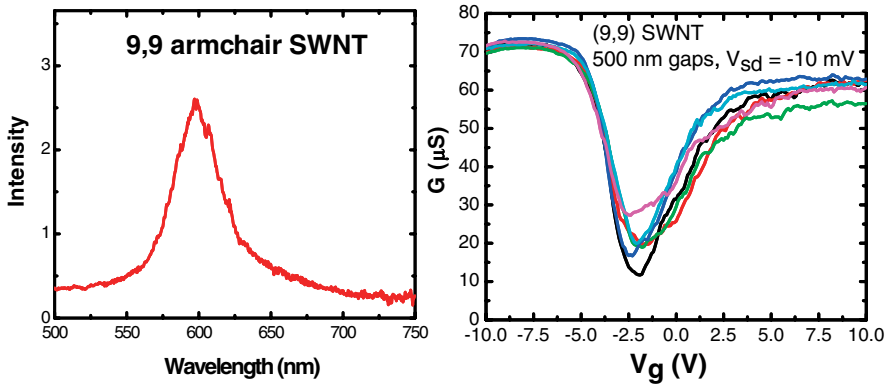

Fig. 3 (online colour at: www.pss-b.com) Optical (left) and transport (right) measurements of a (9, 9) armchair tube.

alignment marks. A small amount of resist is then applied through the back of the slit and cured, so that the suspended section is held firmly down on the target. The two chips are then separated, leaving the ~100 micron nanotube section in place, at which time the resist is gently removed. The top right image in Fig. 2 shows a successfully transferred nanotube between alignment marks on the target chip.

After transfer, electron-beam lithography is used to define contacts in the standard fashion. For these experiments, Pd (25 nm) was used to achieve low contact resistance, with large Cr/Au bonding pads defined in a second lithography step. Because of the length of the transferred tubes, it is possible to put multiple contacts on each one (Fig. 2, bottom).

4 Transport measurements

Using the transfer method, it is possible to measure the three-terminal (source-drain-gate) transport properties of nanotubes of known structure. For this study, the nanotubes were transferred to a degenerately doped Si substrate with a 200 nm insulating SiO_2 layer, so that the Si substrate acted as the back gate. The transport data shown below are low-bias conductance, measured as a function of gate voltage, at room temperature.

Figure 3 shows optical and transport data on a sample identified as a (9, 9) armchair nanotube: the single peak has a position consistent with the M_{11} transition of a 1.25-nm diameter tube. The transport data show quasi-metallic behavior, with finite conductance at all gate voltages. Furthermore, the conductance is high, indicating high-quality contacts, and consistent for all of the devices across the tube (the

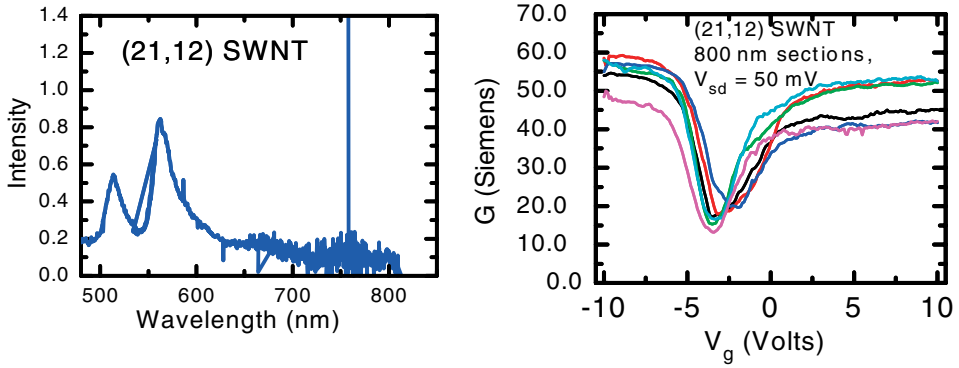

Fig. 4 (online colour at: www.pss-b.com) Optical (left) and transport (right) measurements of a (21, 12) SWNT.

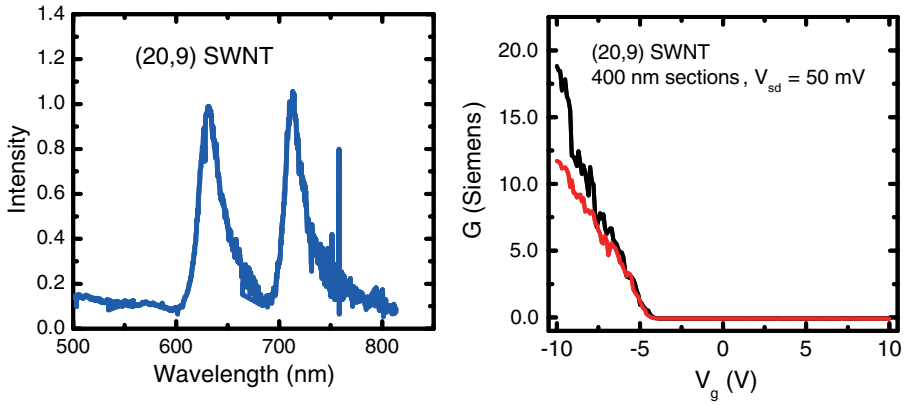

Fig. 5 (online colour at: www.pss-b.com) Optical (left) and transport (right) measurements of a (20, 9) SWNT.

traces for 5 different sections are shown here). However, the conductance dips near zero gate voltage, which is not expected for an armchair tube. The discrepancy might be due to the effects of mechanical strain or resonant scattering from defects, and is the subject of ongoing study.

Figure 4 shows optical and transport data on a sample identified as a (21, 12) nanotube. It shows a split peak whose center position is consistent with the M_{22} transition of a 2.3 nm-diameter tube. Because $n - m = 9$, this tube is expected to be a small-gap semiconductor. The transport data show a small dip in the gate response, consistent with this prediction.

Figure 5 shows an optical spectrum with two distinct peaks indicative of semiconducting structure. The position and peak separation indicate that the structure is (20, 9). Because $n - m = 11$, this tube is expected to be semiconducting. Consistent with this prediction, the conductance vs. gate voltage shows p-type semiconducting behavior, with a large gate voltage dependence and a small off-current. Because of hysteresis effects, the gate voltage swing was limited to ± 10 volts, but similar devices show n-type conduction at high positive gate voltages.

5 Conclusion

We have demonstrated a method for performing three-terminal transport measurements on SWNTs of known crystal structure. Initial data is so far consistent with the predictions of tight-binding theory: nanotubes with $n - m = 3i$ show metallic or quasi-metallic behavior, while others show semiconducting behavior. However, an anomalous dip is observed in the gate response of an armchair nanotube. Further measurements using this technique will permit the full exploration of the relationship between crystal structure and transport.

Acknowledgements This work was supported by the NSF under grant ECS-05-07111. JH and TFH acknowledge additional support from Intel corporation.

References

[1] R. Saito, G. Dresselhaus, and M. S. Dresselhaus, Physical Properties of Carbon Nanotubes (Imperial College Press, Singapore, 2001).
[2] C. L. Kane and E. J. Mele, Phys. Rev. Lett. **78**, 1932–1935 (1997).
[3] P. Kim, T. W. Odom, J. L. Huang, and C. M. Lieber, Phys. Rev. Lett. **82**, 1225–1228 (1999).
[4] Z. H. Chen, J. Appenzeller, J. Knoch, Y. M. Lin, and P. Avouris, Nano Lett. **5**, 1497–1502 (2005).
[5] V. Perebeinos, J. Tersoff, and P. Avouris, Phys. Rev. Lett. **94**, 086802 (2005).
[6] L. Yang, M. P. Anantram, J. Han, and J. P. Lu, Phys. Rev. B **60**, 13874–13878 (1999).

[7] J. Cao, Q. Wang, M. Rolandi, and H. Dai, Phys. Rev. Lett. **93**, 216803 (2004).
[8] J. C. Meyer et al., Appl. Phys. Lett. **85**, 2911 (2004).
[9] M. Kociak et al., Phys. Rev. Lett. **89**, 155501 (2002).
[10] L. Huang, S. J. Wind, and S. P. O'Brien, Nano Lett. **3**, 299–303 (2003).
[11] M. Y. Sfeir et al., Science **306**, 1540–1543 (2004).
[12] S. M. Bachilo et al., Science **298**, 2361–2366 (2002).
[13] J. Maultzsch, H. Telg, S. Reich, and C. Thomsen, Phys. Rev. B **72** (2005).
[14] M. Y. Sfeir et al., Science **312**, 554 (2006).
[15] X. M. H. Huang, R. Caldwell, L. M. Huang, S. C. Jun, M. Y. Huang, M. Y. Sfeir, S. P. O'Brien, and J. Hone, Nano Lett. **5**, 1515–1518 (2005).

